

Remnants from Gamma-Ray Bursts

Shai Ayal and Tsvi Piran

Racah Institute of Physics, Hebrew University, Jerusalem 91904, Israel

ABSTRACT

We model the intermediate time evolution of a “jetted” gamma-ray burst by two blobs of matter colliding with the interstellar medium. We follow the hydrodynamical evolution of this system numerically and calculate the bremsstrahlung and synchrotron images of the remnant. We find that for a burst energy of 10^{51} erg the remnant becomes spherical after ~ 5000 years when it collects $\sim 50M_{\odot}$ of interstellar mass. This result is independent of the exact details of the GRB, such as the opening angle. After this time a gamma-ray burst remnant has an expanding sphere morphology. The similarity to a supernova remnant makes it difficult distinguish between the two at this stage. The expected number of non-spherical gamma-ray burst remnants is ~ 0.05 per galaxy for a beaming factor of 0.01 and a burst energy of 10^{51} erg. Our results suggest that that the double-shell object DEM L 316 is not a GRB remnant.

1. Introduction

If a γ -ray burst (GRB) originate within a galactic disk then the large deposition of energy will result in a blast wave whose initial phase produces the afterglow. The late phase of the blast wave evolution would result, as noted by Chevalier (1974) in the context of supernova remnants (SNRs), in a cool expanding H I shell. The shell will remain distinct from its surrounding until it has slowed down to a velocity of $\approx 10 \text{ km s}^{-1}$. This would happen within $2.3E_{51}^{0.32} 10^6 \text{ yr}$ where E_{51} is the initial energy in units of 10^{51} erg (Loeb & Perna 1998). The current rate of GRBs is one per $\sim 10^7 \text{ yr}$ per galaxy (Schmidt 1999). This leads us to expect a few remnants per galaxy at any given time. However SN are 10^5 times more frequent and it would be difficult to distinguish between a SNR and a GRB remnant. Today there is mounting evidence that some GRBs are beamed (Halpern et al. 1999; Harrison et al. 1999; Kulkarni et al. 1999; Sari 1999; Kuulkers et al. 2000; Salmonson 2000). Beamed GRBs will illuminate only a fraction f_b of the sky, and their rate should be higher by a factor of f_b^{-1} . With $f_b \sim 0.01$ we would expect a hundred GRB remnants per galaxy. At an early stage the morphology of a “jetted” GRB remnant would be very different from a spherical explosion. This can be used to identify those remnants. We study this phase here.

Both beamed GRBs and SN deposit a comparable ($\sim 10^{51}$ erg) energy into the ISM. In both cases the evolution is expected to be similar since both are in the Sedov (Sedov 1959) regime where all the energy is the initial explosion energy and all the mass is in the surrounding ISM. A key

distinguishing feature unique to GRB remnants could be their beamed nature which we expect would lead to a distinct double shell morphology at intermediate times (the late time behavior of the GRB remnant is expected to be spherical in any case). In order to establish how many H I shells are GRB remnants we must find out the expected morphology of GRB remnants and how long they remain non-spherical, and distinguishable from SNRs.

Expanding H I shells have been found in many spiral galaxies (Tenorio-Tagle & Bodenheimer 1988). The interior of these shells is relatively empty and their current expansion velocity is in the order of tens of Km s^{-1} . Models for the origin of these H I supershells involve a large number of spatially correlated supernova events (Heiles 1979, 1984), infall of massive gas clouds on to the galactic plane (Tenorio-Tagle & Bodenheimer 1988) and flaring of radio lobes formed by jets ejected from the galactic nucleus during an active phase (Gopal-Krishna & Irwin 2000). It has been previously noted (Efremov et al. 1998; Loeb & Perna 1998) that a subset of these H I supershells may be the late signature left by GRBs on the interstellar medium (ISM). Establishing how many of the H I shells are GRB remnants would make it possible to directly estimate the local rate of GRBs, determine ϵ , the efficiency of converting the explosion energy into γ -rays, and the beaming factor f_b (Loeb & Perna 1998).

We model the intermediate evolution of a beamed GRB by two blobs of dense material moving into the ISM in opposite directions and we follow numerically their hydrodynamical evolution. Our results can be rescaled to fit a variety of initial energies. We find that at a time of ~ 5000 yr, when the ratio Mc^2/E_0 between the accumulated mass, M , and the initial GRB energy, E_0 , reaches $\sim 9.6 \times 10^4$ the remnant becomes spherical, similar in shape to a SNR. This value is independent of the exact initial details of our model such as the opening angle, the velocity and the morphology. We compare our results to the H I shells DEM L 316 (Williams et al. 1997) previously classified as two colliding SNRs. As the accumulated mass there is much larger it is most likely not a GRB remnant.

We describe our model and the numerical methods in section 2. In section 3 we describe our results. Discussion and summary including a comparison with DEM L 316 are given in section 4.

2. The Simulation

2.1. Model

We study the intermediate evolution of the relativistic ejecta that caused a GRB. We assume that this matter was ejected in the form of two ultra relativistic blobs moving in opposite directions with a bulk Lorenz factor $\Gamma \gtrsim 100$. The emission from internal collisions in the blobs during an early stage comprises the GRB. Late external shocks caused by collisions with circumstellar matter produce the afterglow. The matter slows down during this interaction and its bulk Lorenz factor Γ , decreases. The ejecta stays collimated only until Γ drops below $\sim 1/\theta_0$, at approximately

$3.4(E_{51,\text{iso}}/\rho_{\text{I}})^{1/3}(\theta_0/0.1)^{8/3}$ hr after the GRB, when it has accumulated $10^{-5}E_{51,\text{iso}}(\theta_0/0.1)^2\text{ M}_{\odot}$ of ISM mass (Sari et al. 1999) where θ_0 is the initial angular width, $E_{51,\text{iso}}$ the isotropic energy in units of 10^{51} erg and ρ_{I} is the surrounding ISM density in units of $10^{-24}\text{ gm cm}^{-3}$. Note that in the rest of the paper E_{51} denotes the *actual* energy in units of 10^{51} erg. At this time the matter will start to expand sideways causing, for an adiabatic evolution, an exponential slowing down (Rhoads 1997). The ejecta continues to expand sideways at an almost constant radial distance from the source $R_0 \sim 0.3E_{51}^{1/3}\rho_{\text{I}}^{-1/3}$ pc until it becomes non-relativistic. At this stage, we begin our simulation.

Without a detailed numerical modeling of the relativistic phase of the ejecta we have only an approximate description of how to construct the initial conditions. We expect the angular width of the ejecta to be ~ 1 rad. Additionally we are constrained by Newtonian energy conservation which yields a relation between R_0 , Γ and E_0 :

$$R_0 \sim 0.3E_{51}^{1/3}\rho_{\text{I}}^{-1/3}(v_0/c)^{-2/3}\text{ pc}. \quad (1)$$

The exact shape and energy distribution of the ejecta are uncertain. This may influence the numerical coefficient in Eq. (1). However we show that the intermediate and late evolution of the ejecta are insensitive to these uncertainties in the initial conditions. This is due to the fact that since we are in the Sedov regime, the mass is dominated by the “external” ISM gas which washes out any variations in the initial conditions of the ejecta. This same mechanism will smear out any non-spherical features in a SN explosion, producing spherical SNRs.

We realize these initial conditions by two identical blobs moving in opposing directions into the ISM. The computational space is a cylinder in which the blobs move along the symmetry axis. Both the blobs and the ISM are modeled by a cold $\gamma = 5/3$ ideal gas. The blobs are denser than the ISM. We consider various initial densities, angular widths and shapes of the blobs in order to make sure that these are indeed unimportant in determining the final morphology. In all runs $v_0 \sim c/3$. To evolve these initial conditions we use a hydrodynamic code, neglecting radiative effects.

We note that we have also used the post Newtonian version of our code with the same initial blob velocity of $c/3$. We found that the blobs slow down rapidly and the results were similar to the Newtonian results. Within a few timesteps we have a Newtonian system. In essence this is equivalent to slightly changing the initial shape of the blobs which, as noted before, is insignificant due to the mass dominance of the ISM.

2.2. The Numerical Method

The code we use is based on the Newtonian version of the smooth particle hydrodynamics (SPH) code introduced in Ayal et al. (2001). The code was adapted for the specific problem at hand. The three computationally important features of the problem are the negligible role of gravity, the large amount of stationary gas representing the ISM, and the symmetry. The fact that gravity is unimportant has made the equations very simple and greatly increased the speed of the

code. Implementing single particle time steps allowed us to put in a large volume of stationary gas without making a big impact on the computational time. This way most of the computational effort is invested in the “important” interacting particles. Typically only 0.1% of the particles actually move during each timestep.

The initial conditions are set up so that the blobs are on the z axis with a velocity along the z axis. With these initial conditions there is a rotational symmetry about the z axis and a reflection symmetry about the $x - y$ plane. We implement the reflection symmetry exactly and the rotation symmetry only approximately. The implementation, similar to Libersky et al. (1993), consists of considering only 1/8 (one quadrant) of the computational volume and adding reflecting boundary conditions on the three inner boundaries defined by the $x - y$, $x - z$, and $y - z$ planes. We implement no outer boundary condition since the surrounding gas is very cold and there is almost no pressure so the outer particles gain only a negligible velocity throughout the course of the simulation. The quadrant we evolve consists of 62,800 SPH particles of which only ~ 10 represent the initial blob, again stressing the total mass dominance of the ISM.

The reflecting boundary conditions are implemented using pseudo-particles. At the beginning of each timesteps, all particles which intersect one of the boundaries (In SPH each particle has a finite size called the smoothing length) are reflected about this boundary and added to the simulation as additional pseudo-particles. After this is done for all reflecting boundaries, we calculate all the time derivatives in the usual manner treating all particles in an equal way. When all time derivatives are calculated we delete all the pseudo-particles. Only the “real” particles are then advanced in time. This simple algorithm allows us to implement reflecting boundary conditions using only a small number (typically 10% of the total number of particles for the three boundaries we use) of additional particles.

The use of SPH requires adding some artificial viscosity in order to resolve shocks. We use the standard artificial viscosity (e.g. Monaghan 1992; Benz 1990) consisting of a term analogous to bulk viscosity and a Von Neuman-Richtmyer artificial viscosity term. For the time integration we used a second order Runge-Kutta integrator with an adaptive stepsize control.

3. Results

We choose the initial velocity to be in the range $0.22c$ to $0.33c$, making relativistic effects small. Equation (1) leaves the freedom of choosing two out of the three parameters E_0 , R_0 and ρ_0 , the initial energy, distance and ISM density respectively. In presenting the results we choose E_0 and ρ_0 . To parameterize the evolution of the remnant we utilize the fact that mass scales linearly with the initial energy and we define the dimensionless parameter $\mu = Mc^2/E_0$ where M is the accumulated shell mass. We define M as all mass with density above $2\rho_0$ corresponding to the shocked material of the shell and to the accumulated ISM mass. All subsequent results are presented as functions of μ . Our simulation begins approximately 2 years after the burst, when $\mu \sim 18$. In Figure 1, we

show the linear scaling of time with μ . The scaling relation is $t \sim 0.053\mu(E_{51}/\rho_I)^{-1/3}$ yr which is close to the Sedov-Taylor (Sedov 1959) blast wave result of $t \propto R^{5/2} \propto \mu^{5/6}$ where R is the radius of the blast wave.

A bow shock forms as each blob collides with the ISM. The shock also propagates in the direction perpendicular to the blob's velocity and over time, backwards. The expected morphology of the remnant will therefore be of two expanding shells which will eventually join, producing yet another shock. At late times the shells will merge and become a single spherical shell. We made several runs, differing in the initial density, shape, initial velocity, angular width and the numerical coefficient in Eq. (1) of the ejecta as summarized in Table 1. In five runs the initial ejecta was shaped like a disk and in one case it was shaped like a sphere. As we show in Fig. 2, for $\mu \gtrsim 5 \times 10^3$ the z positions of the shock and its maximal radius in the $x - y$ plane, r_{xy} are indeed unaffected by these variations in initial conditions. The μ at which the shells touch depends on the exact initial conditions, but all other events (such as the μ at which the remnant becomes spherical) are unaffected. Therefore in the following discussions we will consider only one of the runs.

The mass inside the shell, defined as all mass with density below $\rho_0/2$ also evolves almost linearly with μ (Fig. 3) as $0.06(E_0/c^2)\mu$. In Fig. 4, we show the density contours as a function of μ . The two shells touch and a shock forms along the equatorial plane between them at $t \sim 50 - 260(E_{51}/\rho_I)^{-1/3}$ yr when $\mu = 1 - 5 \times 10^3$ depending on the initial conditions. The maximal z position of the shock and r_{xy} can be fitted with a power law as shown in Fig. 5. The scaling relation for r_{xy} is $r_{xy} = 0.07\mu^{0.45}(E_{51}/\rho_I)^{1/3}$ pc $\propto t^{0.45}$. The effective radius of the shell, $(r_{xy}^2 z)^{1/3}$, scales as $t^{0.4}$, exactly the result expected for a Sedov-Taylor blast wave. The ratio z_{max}/r_{xy} decreases in time staying always between 1 and 2 (see Fig 6). Extrapolating we see that this ratio reaches a value of 1 at $\mu \sim 9.6 \times 10^4$. At this time the shock has a spherical shape with $z = r_{xy} \sim 12(E_{51}/\rho_I)^{1/3}$ pc. Even then the shock will not be completely spherically symmetric as there would still be a ring of shocks around the “equator” where the shells have collided.

During the whole run, total energy is conserved to within 1%. In Fig. 7 we show E_z the total kinetic energy in the z direction, E_{xy} the total kinetic energy in the $x - y$ plane and E_i the total internal energy in the simulated volume. As the blobs interact with the ISM E_i and E_{xy} increase at the expense of E_z . E_{xy} increases until $\mu \sim 5 \times 10^3$ and then it remains constant at $0.22E_0$. E_i increases by a factor of 200 to a value of $0.72E_0$, most of the increase occurs before $\mu \sim 2500$. In the final configuration ($\mu \sim 2 \times 10^4$) 72% of the energy is in internal energy, 22% is in kinetic energy in the $x - y$ plane and only 6% remains in the kinetic energy in the z direction.

Figures 8 and 9 depict the images of the remnant as a function of time and angles of inclination. We show images due to bremsstrahlung emission and synchrotron emission. The images are constructed assuming that all the gas is optically thin in the relevant frequencies. The bremsstrahlung luminosity (Fig. 8) was calculated assuming that the volume emissivity is proportional to $\rho^2 \varepsilon^{1/2}$ (Lang 1980). In calculating the synchrotron emissivity (Fig. 9) we assumed that both the magnetic field energy density and the energy of the relativistic electrons are proportional to the internal en-

ergy density of the gas with the proportionality factors ϵ_B and ϵ_e respectively. We further assume that the relativistic electron number density is a power law in energy. Under these assumptions the volume emissivity is proportional to $\rho^2 \epsilon^2$ (e.g. Shu 1991). In the late images there are two bright circles at the lines where the colliding blobs forming a hot shocked region.

4. Discussion

We follow the hydrodynamic evolution of two blobs colliding with the ISM. This scenario is a model for the intermediate time behavior of matter ejected from a central engine producing a GRB. Our results can be rescaled to fit a variety of initial energies and ISM densities. The two shells touch and a shock forms along the equatorial plane between them at $t \sim 50 - 160(E_{51}/\rho_I)^{-1/3}$ yr when $\mu = 1 - 5 \times 10^3$. We show that the late time remnant is insensitive to the exact initial morphology, angular width and density of the ejecta. Although initially the remnant may be highly non-spherical, the ratio between its height and radius will approach unity and it will eventually become spherical in shape after a time of $\sim 5 \times 10^3 E_{51}^{1/3} \rho_I^{-1/3}$ yr when $\mu \gtrsim 9.6 \times 10^4$. After this time it will be difficult to distinguish a GRB remnant from a SNR using the morphology. The expected number of non-spherical GRB remnants is, therefore, $5 \times 10^{-4} f_b^{-1} E_{51}^{1/3} \rho_I^{-1/3}$ per galaxy (using the observed present GRB rate (Schmidt 1999) of 10^{-7} yr $^{-1}$ gal $^{-1}$).

The results of Gaensler (1998) show a tendency for the bilateral axis of the non-spherical SNRs to be aligned with the galactic plane. This presents strong evidence in favor of an extrinsic model for the origin of non-spherical SNRs. Using our results, we can propose an alternative explanation to the origin of some of the highly non-spherical SNRs and H_I shells. Instead of assuming an *extrinsic* model, namely spherical energy deposition into a non isotropic medium we propose an *intrinsic* model: non spherical energy deposition into an isotropic medium. Our GRB remnant model can explain non-spherical SNRs with a two shell morphology provided that $\mu \lesssim 9.6 \times 10^4$. One extreme and well studied case, the non-spherical SNR DEM L 316 (Williams et al. 1997), has a distinct double shell morphology. The external model clearly fails here. However the ratio μ measured for DEM L 316 is $\gtrsim 7.1 \times 10^5$ and a GRB remnant would already be spherical at this stage, suggesting that DEM L 316 is not a GRB remnant. This conclusion could be revised if for some reason the initial blobs stay confined for a much longer period (so that eq. 1 is not satisfied) or if the solution becomes radiative before becoming spherical and the radiative cooling slow down the evolution.

We thank the anonymous referee for his helpful comments. This research was supported by a ISRAEL-US BSF grant.

REFERENCES

Ayal, S., Piran, T., Oechslin, R., Davies, M. B., & Rosswog, S. 2001, *ApJ*, in press

Benz, W. 1990, in *The Numerical Modeling of Nonlinear Stellar Pulsations: Problems and Prospects*, ed. J. R. Buchelr (Dordrecht: Kluwer), 269–288

Chevalier, R. A. 1974, *ApJ*, 188, 501

Efremov, Y. N., Elmegreen, B. G., & Hodge, P. W. 1998, *ApJ*, 501, L163

Gaensler, B. M. 1998, *ApJ*, 493, 781+

Gopal-Krishna & Irwin, J. A. 2000, *A&A*, in press

Halpern, J. P., Kemp, J., Piran, T., & Bershadsky, M. A. 1999, *ApJ*, 517, L105

Harrison, F. A., Bloom, J. S., Frail, D. A., Sari, R., Kulkarni, S. R., Djorgovski, S. G., Axelrod, T., Mould, J., Schmidt, B. P., Wieringa, M. H., Wark, R. M., Subrahmanyam, R., McConnell, D., McCarthy, P. J., Schaefer, B. E., McMahon, R. G., Markze, R. O., Firth, E., Soffitta, P., & Amati, L. 1999, *ApJ*, 523, L121

Heiles, C. 1979, *ApJ*, 229, 533

—. 1984, *ApJS*, 55, 585

Kulkarni, S. R., Djorgovski, S. G., Odewahn, S. C., Bloom, J. S., Gal, R. R., Koresko, C. D., Harrison, F. A., Lubin, L. M., Armus, L., Sari, R., Illingworth, G. D., Kelson, D. D., Magee, D. K., van Dokkum, P. G., Frail, D. A., Mulchaey, J. S., Malkan, M. A., McClean, I. S., Teplitz, H. I., Koerner, D., Kirkpatrick, D., Kobayashi, N., Yadigaroglu, I. ., Halpern, J., Piran, T., Goodrich, R. W., Chaffee, F. H., Feroci, M., & Costa, E. 1999, *Nature*, 398, 389

Kuulkers, E., Antonelli, L. A., Kuiper, L., Kaastra, J. S., Amati, L., Costa, E., Frontera, F., Heise, J., in 't Zand, J. J. M., Masetti, N., Nicastro, L., Pian, E., Piro, L., & Soffitta, P. 2000, *ApJ*, 538, 638

Lang, K. R. 1980, *Astrophysical Formulae* (Springer-Verlag)

Liberky, L. D., Petschek, A. G., Carney, T. C., Hipp, J. R., & Allahdadi, F. A. 1993, *J. Comp. Phys.*, 109, 67

Loeb, A. & Perna, R. 1998, *ApJ*, 503, L35

Monaghan, J. J. 1992, *ARA&A*, 30, 543

Rhoads, J. E. 1997, *ApJ*, 487, L1

Salmonson, J. D. 2000, *ApJ*, 544, L115

Sari, R. 1999, in Proc. of the 5th Huntsville Gamma-Ray Burst Symposium

Sari, R., Piran, T., & Halpern, J. P. 1999, ApJ, 519, L17

Schmidt, M. 1999, ApJ, 523, L117

Sedov, L. I. 1959, Similarity and Dimensional Methods in Mechanics (New York: Academic Press)

Shu, F. H. 1991, The Physics of Astrophysics, Vol. 1 (University Science Books)

Tenorio-Tagle, G. & Bodenheimer, P. 1988, ARA&A, 26, 145

Williams, R. M., Chu, Y. H., Dickel, J. R., Beyer, R., Petre, R., Smith, R. C., & Milne, D. K. 1997, ApJ, 480, 618+

This preprint was prepared with the AAS L^AT_EX macros v5.0.

run	shape	angular width	density [ρ_I]
1	disc	10/3	6/5
2	disc	1	4/3
3	disc	2	3
4	disc	1	3
5	disc	7/12	3
6	sphere	1/2	2

Table 1: Initial parameters for the different runs. Initial density is in units of ρ_I .

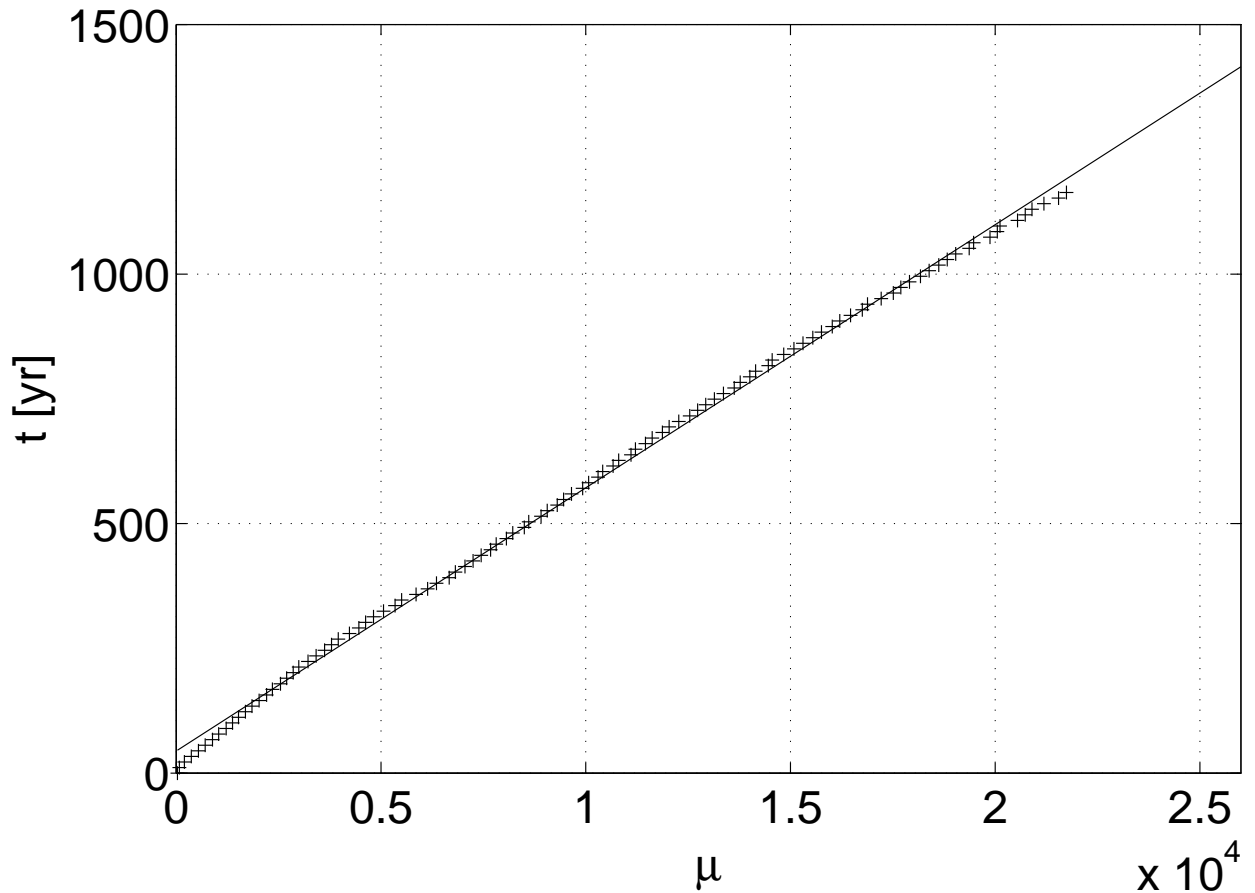


Fig. 1.— Time as a function of μ . The linear relation between time and μ is $t \sim 0.046\mu(E_{51}/\rho_1)^{-1/3}$ yr. In this and all subsequent figures the results are presented for an initial energy of 10^{51} erg and ISM density of 10^{-24} gm cm $^{-3}$.

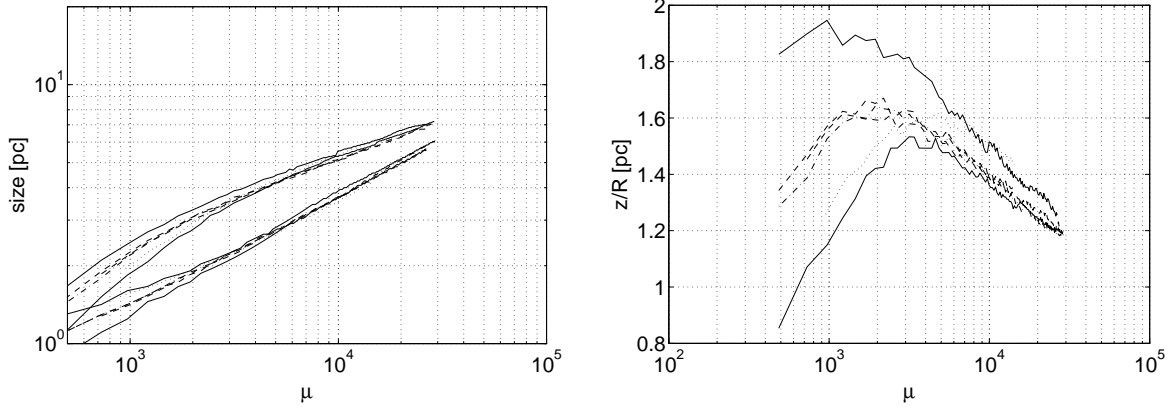


Fig. 2.— Comparison of the various runs showing their similarities. (a) The z and r_{xy} positions of the shocks (the z positions are the higher lines). (b) The ratio z/r_{xy} for all the runs.

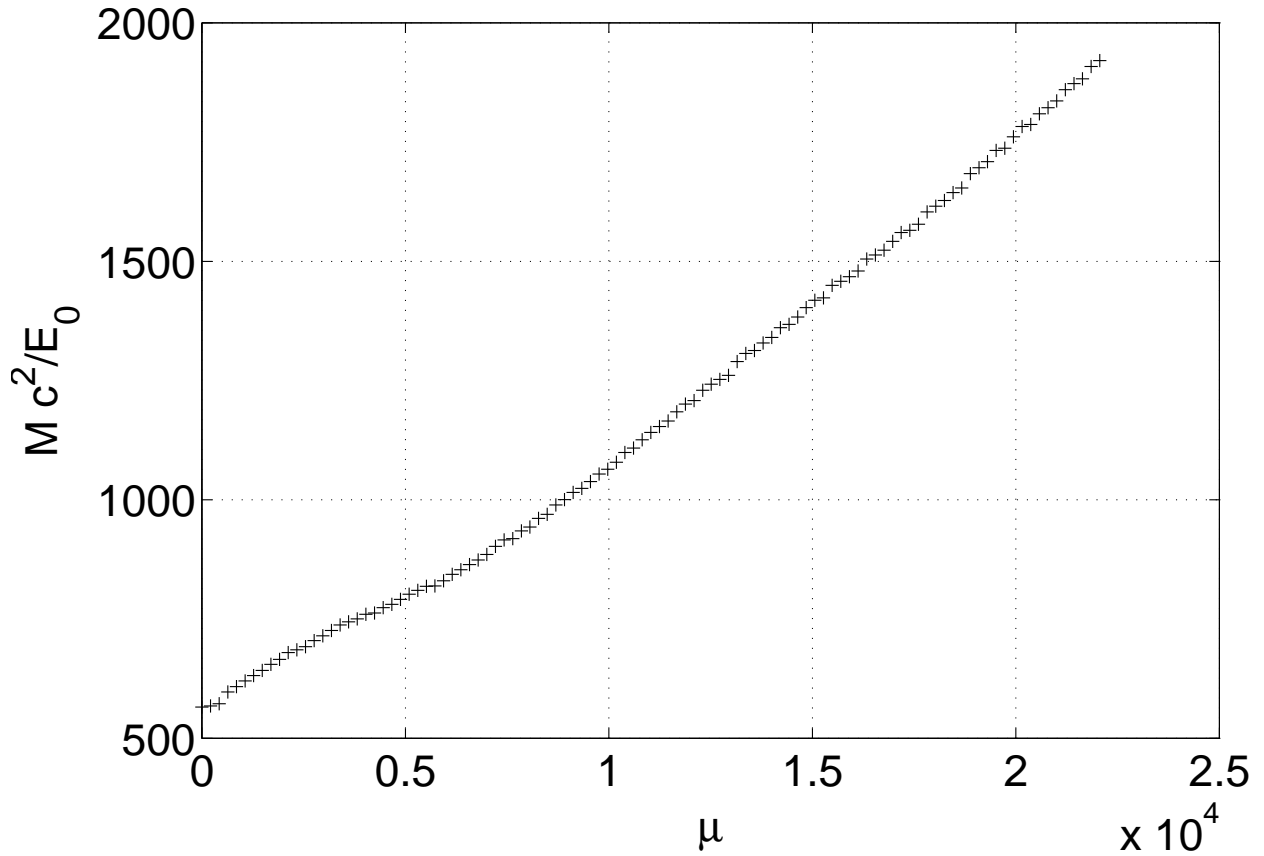


Fig. 3.— Mass inside the shell as a function of μ .

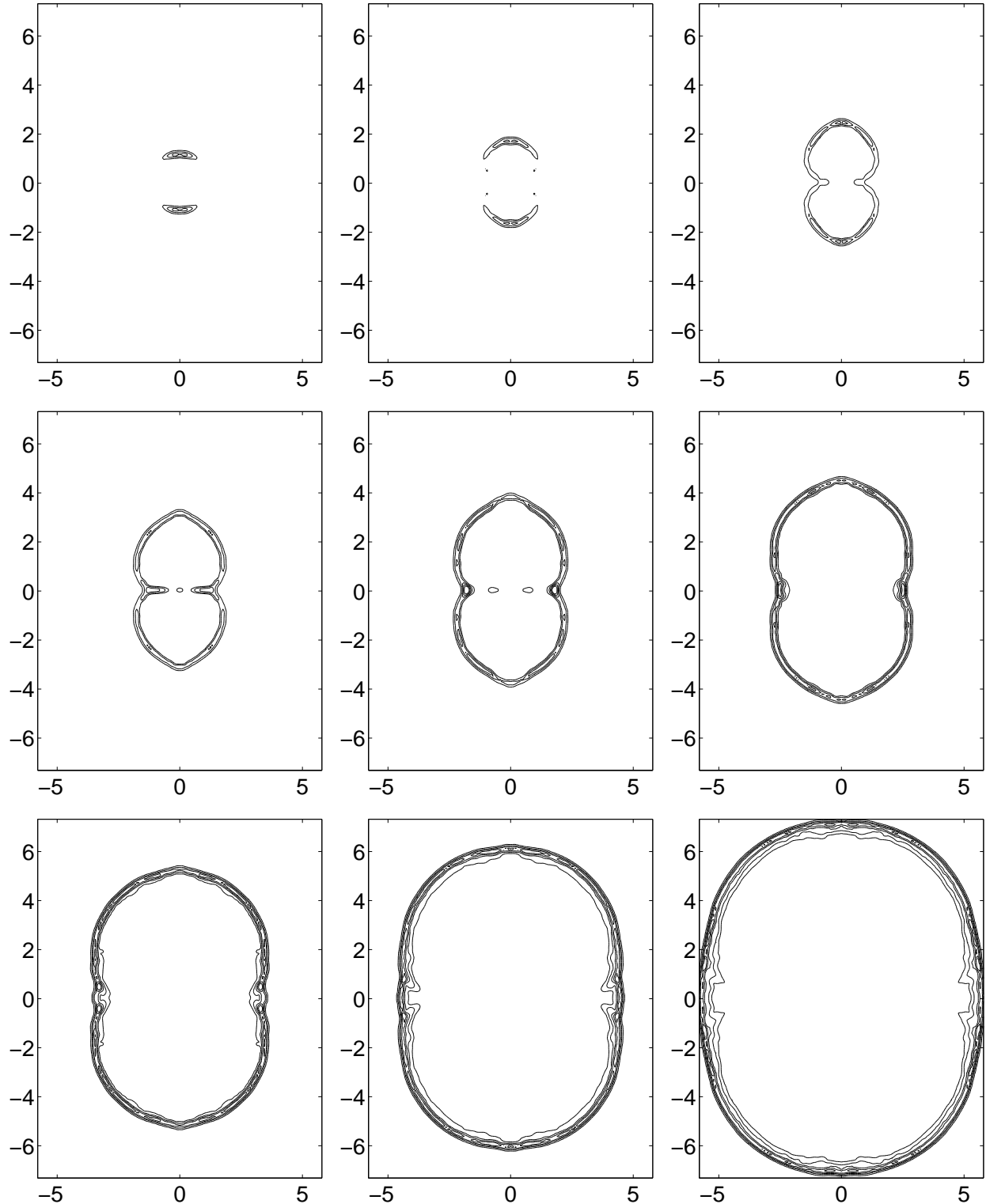


Fig. 4.— Density contours. The length scale is in pc. Contours are equal spaced at $1.5\rho_0, 2\rho_0, \dots, 3.5\rho_0$. The images are at $\mu = 2.1 \times 10^2, 4.2 \times 10^2, 8.5 \times 10^2, 1.5 \times 10^3, 2.5 \times 10^3, 4.5 \times 10^3, 7.6 \times 10^3, 1.3 \times 10^4, 2.2 \times 10^4$ (left to right, top to bottom)

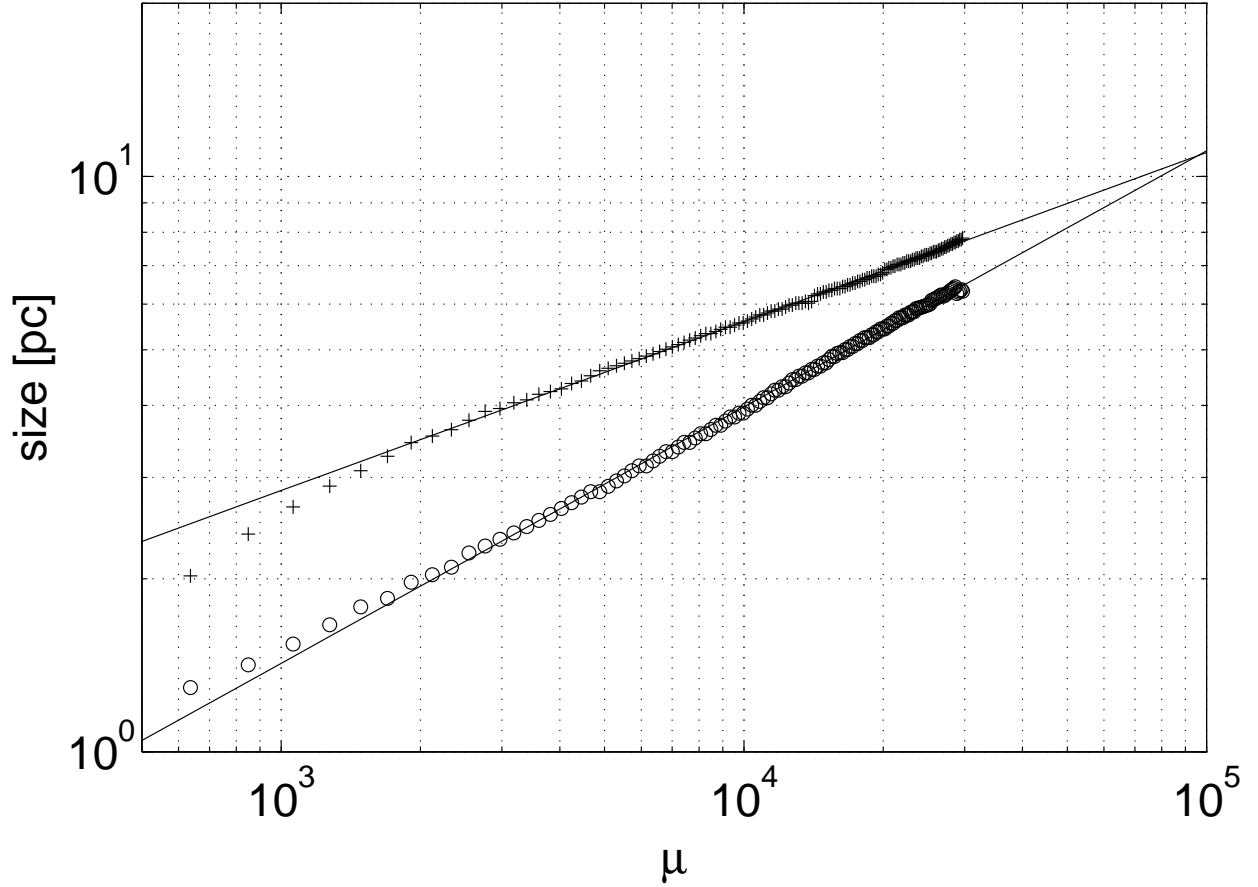


Fig. 5.— log-log plot of the z position of the blobs (crosses) and the maximum radius in the $x - y$ plain of the shock r_{xy} (circles) as a functions of μ . The solid lines are the best fit power laws for $\mu > 2200$ which are $z \propto \mu^{0.29}$ and $r_{xy} \propto \mu^{0.45}$. The lines are extrapolated to the point where they cross at $\mu \sim 9.6 \times 10^4$

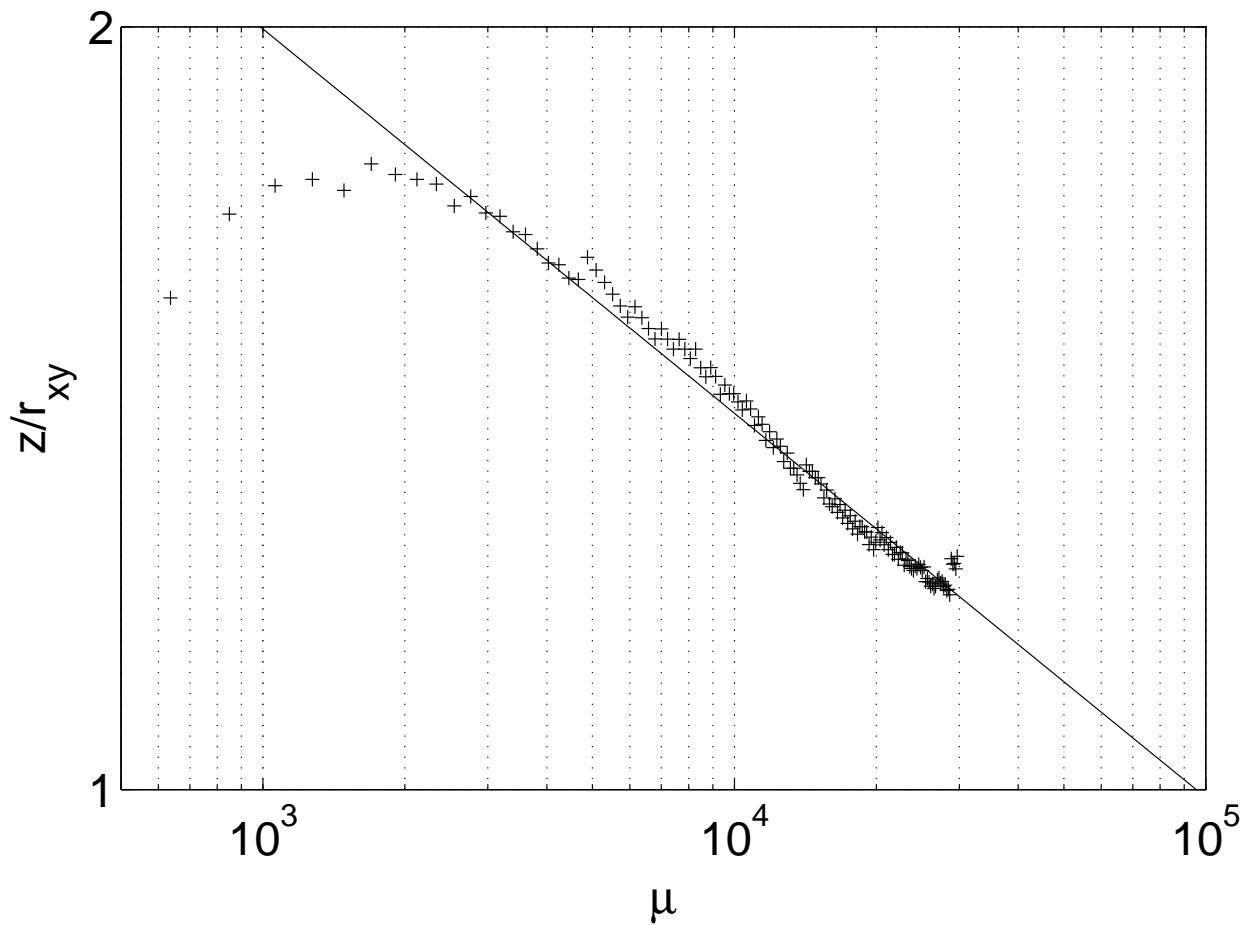


Fig. 6.— The ratio between the radius r_{xy} of the shock and the z position of the shock. The solid line is the best fit power law $\mu^{-0.15}$. The ratio will reach a value of 1 at $\mu \sim 9.6 \times 10^4$ yr

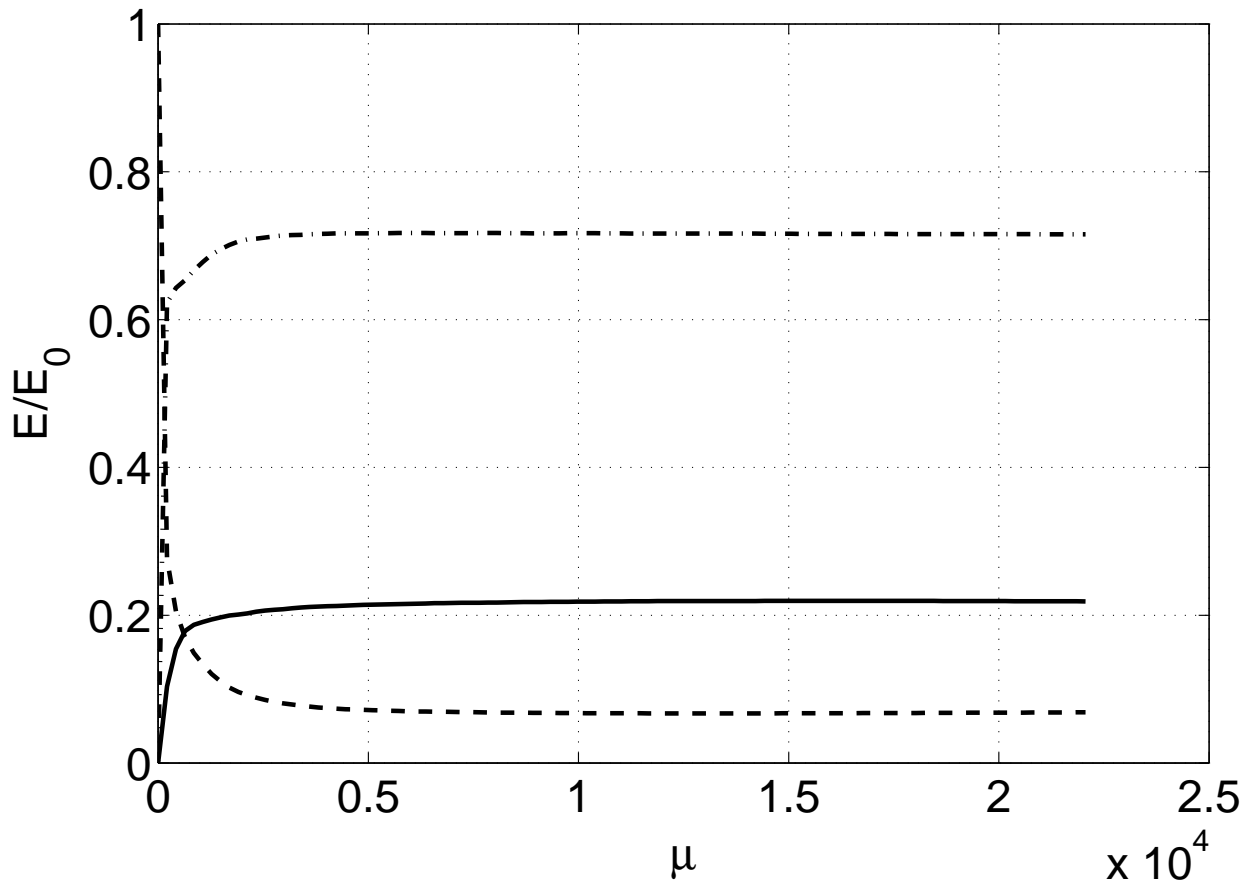


Fig. 7.— plot of total kinetic energy in the z direction (dashed line), total kinetic energy in the $x-y$ direction (solid line) and total internal energy (dash-dotted line). The energies are scaled by the initial kinetic energy E_0 .

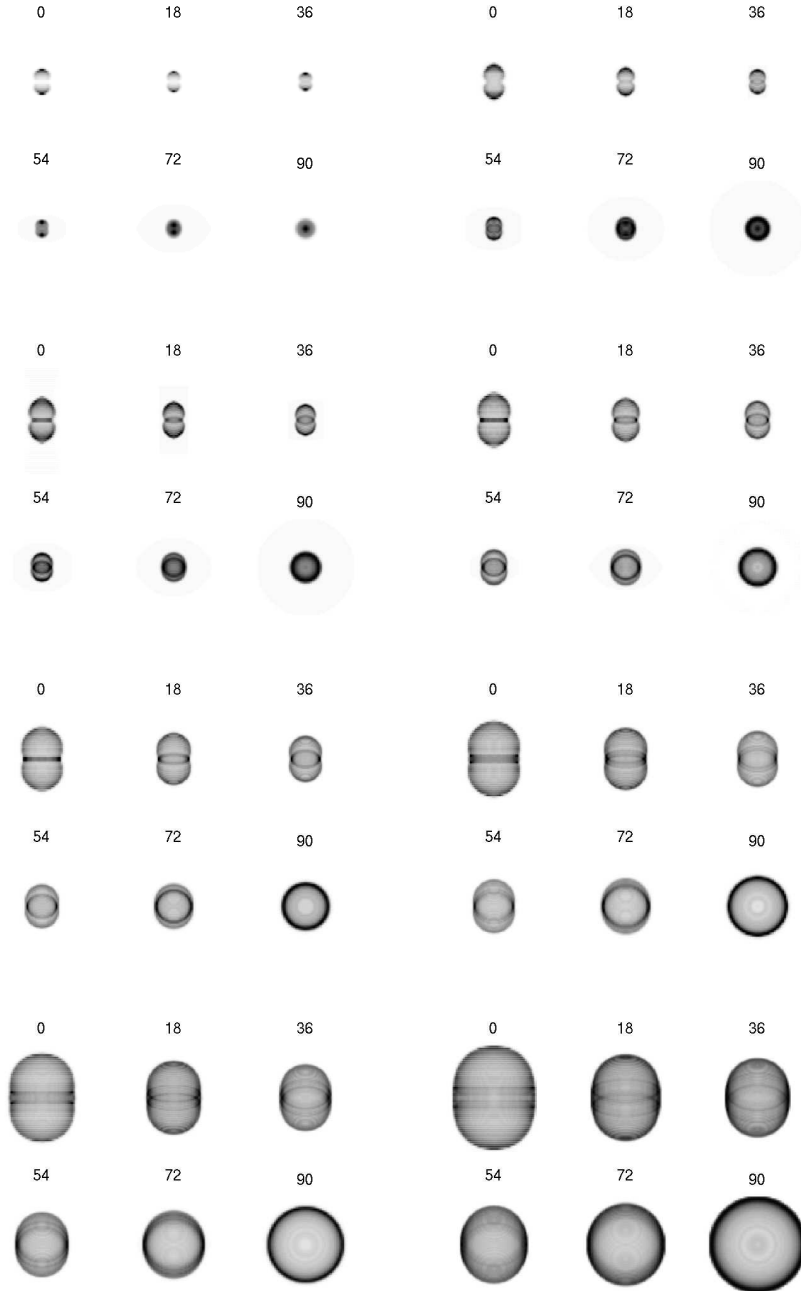


Fig. 8.— Images of the remnant, bremsstrahlung emission. The number above each image is the angle of inclination in degrees. The images are shown at the same μ as the last 8 panels of figure 4.

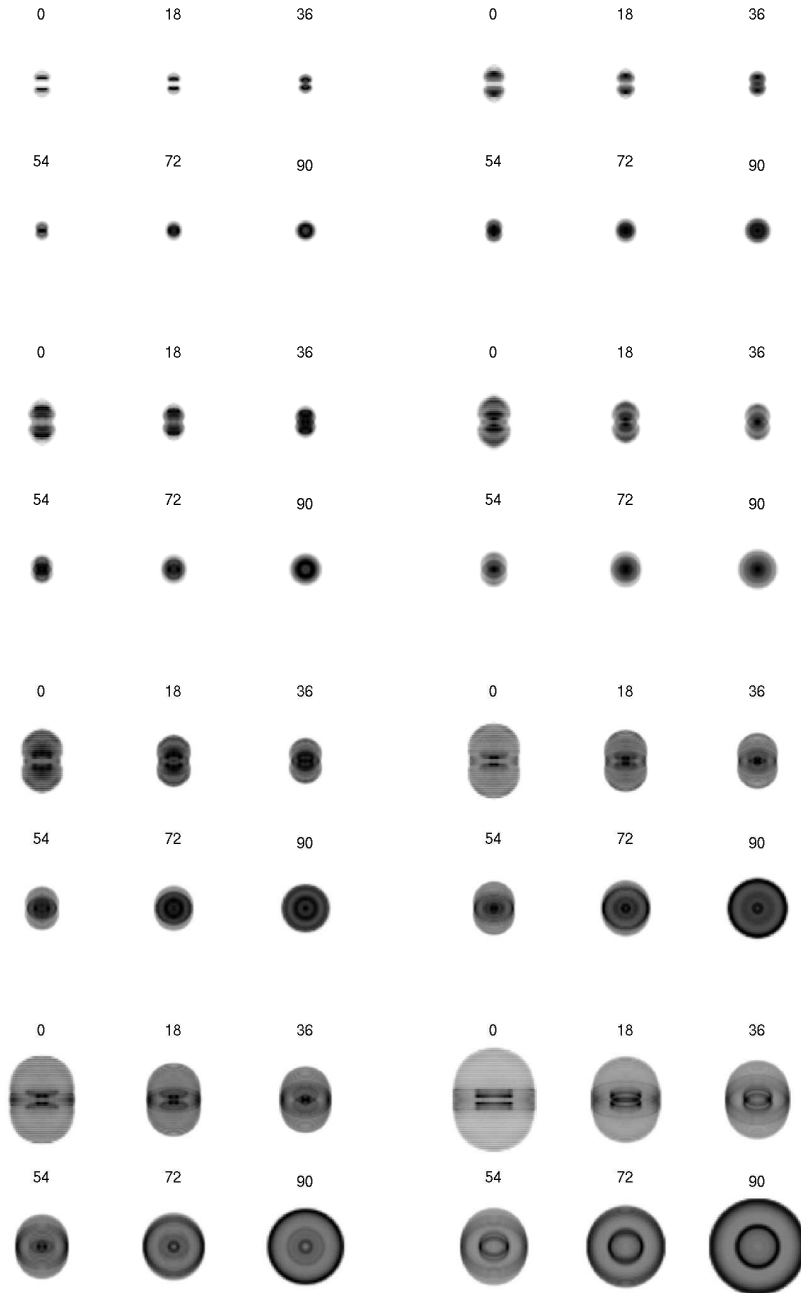


Fig. 9.— Images of the remnant, synchrotron emission. The μ are the same as the last 8 panels in figure 8